

Experimental analysis of concrete behavior under high confinement: Effect of the saturation ratio

Xuan Hong Vu^{a,*}, Yann Malecot^a, Laurent Daudeville^a, Eric Buzaud^b

^a Université Joseph Fourier – Grenoble I, Laboratoire 3S-R, CNRS, INPG, BP53, 38041 Grenoble Cedex, France

^b DGA, Centre d'Etudes de Gramat, 46500 Gramat, France

ARTICLE INFO

Article history:

Received 23 February 2008

Received in revised form 7 October 2008

Available online 25 October 2008

Keywords:

Concrete

Saturation ratio

Triaxial test

High confinement

ABSTRACT

This study focuses on the identification of concrete behavior under severe triaxial loading in order to better evaluate the vulnerability of sensitive infrastructure to near-field detonations or ballistic impacts. For the purpose of reproducing high stress levels with well-controlled loading paths, static tests have been conducted on concrete samples using a triaxial press offering very high capacities (stress levels of around 1 GPa). It is a well-known fact that the concrete drying process is a slow phenomenon. Massive concrete structures, such as bridge piers, dams and nuclear reactors, could retain a quasi-saturated core throughout most of their lifetime, even though their facing dries very quickly. The objective of this article is to evaluate the effect of the saturation ratio on concrete behavior under high confinement; this article will present triaxial test results on concrete samples over a saturation ratio range extending from dried to quasi-saturated concretes. The subsequent analysis of results will show that the saturation ratio exerts a major influence on concrete behavior, particularly on both the concrete strength capacity and shape of the limit state curve for saturation ratios above 50%. This analysis also highlights that while the strength of dried concrete strongly increases with confining pressure, it remains constant over a given confining pressure range for either wet or saturated samples.

© 2008 Elsevier Ltd. All rights reserved.

1. Introduction

Severe dynamic loading, such as that produced by near-field detonation or ballistic impacts on a concrete infrastructure, can generate very high-intensity triaxial stress states in concrete material. During these solicitations, the concrete is subjected to various kinds of loading paths, associated with different damage modes (Zukas, 1992; Bailly et al., 1996). The validation of concrete behavior models, which simultaneously take into account the phenomena of brittle damage and irreversible strain (e.g. compaction), thus requires test results that enable reproducing complex loading paths.

Most experimental results available in the literature only pertain to triaxial loadings with a moderate level of confining pressure (Li and Pugh, 1970; Kupfer and Gerstle, 1973; Wang et al., 1987; Jiang et al., 1991; Imran and Pantazopoulou, 1996; Taliercio et al., 1999; Sfer et al., 2002). In particular, these authors have revealed the transition from brittle to ductile behavior that characterizes cohesive materials. Many studies have shown that dynamic tests on concrete, e.g. using split Hopkinson pressure

bars (Hopkinson, 1914; Zhao and Gary, 1996), are rather difficult to perform, primarily due to the brittle nature of the material, which then leads to failure during the transient loading stage. The inhomogeneous characteristic of the sample stress state, along with very limited control over the loading path and relatively poor instrumentation, contributes to complicate test result interpretation. However, test results available in the literature show concrete strength to be an increasing function of the loading rate. This dependence of concrete behavior on loading rate under compression loading seems to be quite small in the absence of a liquid phase (Bischoff and Perry, 1991; Toutlemonde, 1995), yet proves to be much higher on traction, as explained to a great extent by the influence of defects (Hild et al., 2003). It has also been shown that rate effects in dynamic uniaxial tensile loading are much higher for wet samples than for dried ones (Rossi et al., 1994). The dynamic triaxial behavior of concrete has not been studied in depth. Confined Hopkinson bar tests have been investigated by Schmidt on concrete samples up to 7-MPa confining pressures. These tests reveal a decrease in concrete response sensitivity to the loading rate as confinement increases (Schmidt, 2003).

Loading rates can be raised by means of the plate impact technique (Le Vu et al., 1996); this type of experiment allows identification of the material equation of state (i.e. pressure–volume relation) at stress levels on the order of several GPa.

* Corresponding author. Tel.: +33 456528634; fax: +33 476827043.

E-mail addresses: vu@hmg.inpg.fr (X.H. Vu), yann.malecot@ujf-grenoble.fr (Y. Malecot), daudevil@ujf-grenoble.fr (L. Daudeville), eric.buzaud@dga.defense.gouv.fr (E. Buzaud).

The results presented in this article make reference to static triaxial tests carried out on concrete samples using a high-capacity hydraulic triaxial press, called the “GIGA” press. Such an experimental device enables reaching stress levels in the samples of around 1 GPa with static, homogeneous and well-controlled loading paths.

Deriving the static characterization of a constitutive model in order to predict dynamic behavior is a well-established practice in the study of geomaterials, yet previous experimental work has essentially been limited to small mortar samples (Bazant et al., 1986; Buzaud, 1998; Burlion et al., 2001; William et al., 2005; Forquin et al., 2007). Such studies emphasize the increase in maximum deviatoric stress of the mortar as well as the evolution in mortar limit states with confinement. The aim of the present paper is to extend this practice to the study of “actual” concrete materials (i.e. with an aggregate dimension on the order of a centimeter).

The comparative study between concrete and mortar with a confining pressure of 500 MPa, as conducted by Akers (Akers and Phillips, 2004), highlights the differences in behavior between those two materials. Moreover, it shows that a study of mortar behavior under high confinement is not representative of concrete behavior. Other triaxial test results on ordinary concrete with confining pressures ranging between 0 and 500 MPa yield the evolution in concrete behavior and limit state with confinement (Schmidt, 2003; Warren et al., 2004).

In 2004, the 3S-R Laboratory launched in collaboration with the Centre d'Etudes de Gramat (Délégation Générale pour l'Armement, French Ministry of Defense, General Delegation for Ordnance) a research program on the vulnerability of concrete infrastructure. In an earlier stage of this program, using the same baseline material, Gabet studied the influence of loading path on concrete behavior (Gabet et al., 2008). In particular, these results displayed that under high confinement, the concrete limit state remains relatively independent of both the loading path and Lode's angle. Once again, using the same baseline material, this paper will present experimental results with respect to the saturation ratio effect on concrete behavior. During a latter stage of this research program, the strain rate effects with different saturation ratios will be studied by means of both split Hopkinson pressure bar and plate impact tests conducted on concrete samples.

Once the cement has set, an ordinary concrete becomes a quasi-saturated material. In most cases, it is then submitted to an environment with lower relative humidity, such that a drying process occurs within the concrete. Since the pore network of the cement matrix is very thin, this moisture transport proceeds very slowly and can be described using a diffusion-like equation (Baroghel-Bouny et al., 1999). The time required to reach moisture equilibrium varies with the square of the built structure thickness. Given that most sensitive concrete infrastructure such as bridge piers, dams and nuclear reactors are very massive, their core could remain quasi-saturated throughout most of their lifetime, even though their facing dries very quickly. The dependence of concrete behavior on saturation ratio thus constitutes an important factor to investigate.

The saturation ratio effect for a cementitious material (concrete and mortar) on its behavior in uniaxial compression has been studied extensively. As the saturation ratio of the material increases, its ultimate stress drops (Pihlajavaara, 1974; Brooks and Neville, 1977; Okajima et al., 1980; Torrenti et al., 1997; Yurtdas et al., 2004a; Burlion et al., 2005) and both its Young's modulus and Poisson's ratio rise (Toutlemonde, 1995; Brooks and Neville, 1977; Yurtdas et al., 2004a; Burlion et al., 2005). For the case of drying shrinkage, the presence of water has a significant influence on the mechanical behavior of concrete, and actually models should include this aspect as discussed for example in the study of Van Mier (Van Mier, 2007). Triaxial tests conducted on cementitious

material samples with a controlled saturation ratio are rarer; a number of triaxial tests and hydrostatic tests with confinement of up to 60 MPa have been carried out by Yurtdas (Yurtdas et al., 2004a) on mortar samples at various degrees of drying. These tests have confirmed the trend observed in uniaxial compression. The drying of mortar increases its strength (maximum deviatoric stress) while decreasing its compressibility modulus and axial stiffness. Moreover, the rise in confining pressure tends to widen disparities in resistance between dried samples and saturated samples (Yurtdas et al., 2004b). At higher levels of mean stress (up to 600 MPa), oedometric tests on mortar samples with different saturation ratios (although not measured) have been performed by Burlion (Burlion et al., 2001; Burlion et al., 1998). Results show that under undrained conditions, a higher water quantity contained within the mortar translates into lower compressibility.

To the best of our knowledge, no results are available regarding the saturation ratio effect on concrete behavior when subjected to extreme static triaxial loading. The objective of the present article then is to compensate for this lack of knowledge, which in fact is due to the difficulty of reproducing such a loading with simultaneous control of concrete moisture content. The experimental device used in this study will be described in the next section. The results of triaxial tests conducted on an ordinary concrete will then be presented for a range of saturation ratios from 11% (dried concrete) to 100% (saturated concrete) and for a confining pressure of up to 650 MPa. The analysis of results will first be provided in terms of stress–strain curves (Section 3) and then in terms of volumetric and deviatoric behavior curves (Sections 4 and 5). The limit state curves relative to the concrete saturation ratio will be displayed in Section 6. The concluding section of this study will demonstrate the major influence of saturation ratio on concrete behavior.

2. Experimental set-up

2.1. The triaxial cell

A high-capacity triaxial press has been specially designed for purposes of this study (Thiot, 2004). The development of a testing procedure on concrete, which has proven rather complex, has been presented in detail in Vu's Ph.D. thesis (Vu, 2007). Fig. 1 shows a general view of the press. A cross-section of the confining cell is provided in Fig. 2. This press is able to generate a confining pressure of up to 0.85 GPa and an axial stress reaching 2.3 GPa on cylindrical concrete specimens 7 cm in diameter and 14 cm long (see Fig. 3). The concrete specimen is placed in the confining cell, and the confining fluid, diethylhexyl azelate – a non-volatile organic liquid, is injected into the cell through the upper opening. The cell is then pressurized by means of a multiplying jack. The axial force is generated from a 13-MN jack placed underneath the cell; this force is transmitted to the specimen via a piston that passes through the lower cell plug. An axial displacement sensor located on the machine is used to control axial jack displacement, while an axial load sensor and pressure sensor positioned inside the confining cell yield the stress state on the specimen. Both the confining pressure and jack axial displacement are servo-controlled, which offers several potential loading paths.

2.2. Strain measurements

Strain measurements are performed by use of an LVDT (linear variable differential transformer) axial sensor, along with one axial and two circumferential gauges (see Fig. 4). The gauges used for this study, EP-08-10CBE-12 type from Vishay Micro-measurements Company, are 28 mm long, i.e. about three times the size

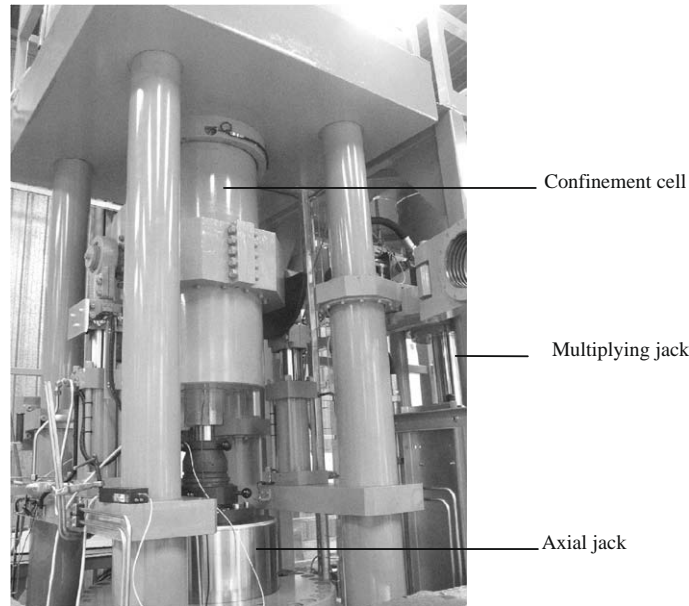


Fig. 1. General view of the GIGA press.

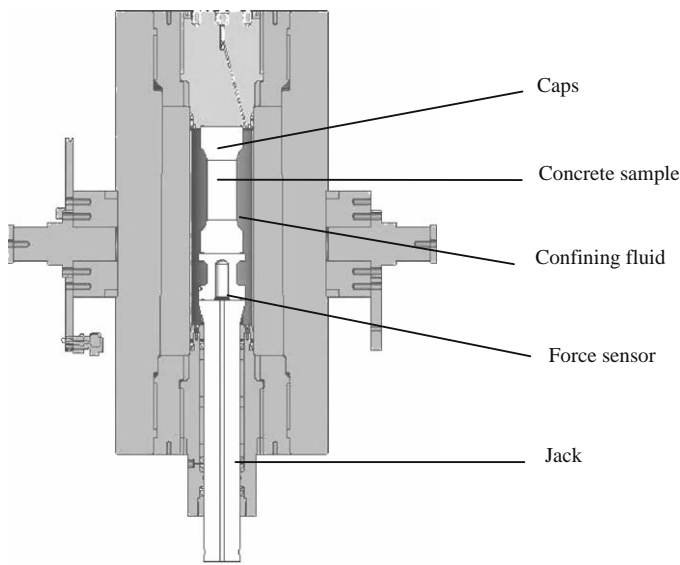


Fig. 2. Cross-section view of the confinement cell.

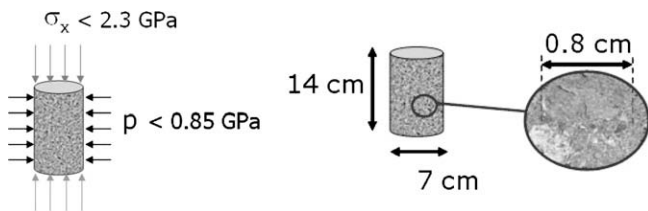


Fig. 3. Maximum press capacity and associated sample sizes of the triaxial cell.

of the largest aggregate. These gauges allow strain measurements up to 15%. The LVDT sensor used for this study, 500XS-3013 type from Schaevitz Sensors Company, consists of a transformer and of a movable magnetic core. Each part of the LVDT sensor is fixed on a loading head. It permits to measure a relative displacement up to 50 mm.

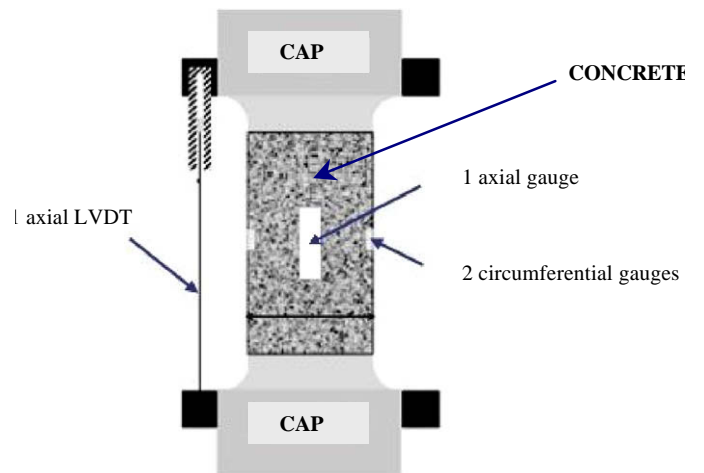


Fig. 4. Schematic diagram of the strain measurement procedure conducted on the sample.

The axial gauge yields a local measurement whereas the LVDT gives a global measurement of the axial strain. The comparison between these two measurements allows a rough evaluation of the sample strain homogeneity. The circumferential strain is measured by means of two diametrically-opposite gauges, such that the probability of maintaining a measurement until the end of the test increases. These two gauges also allow another control of the strain homogeneity. The use of gauges on concrete for triaxial compression tests in the presence of such high confinement levels represents, to the best of our knowledge, a completely novel approach.

2.3. Sample protection

Given the porous nature of concrete, this high level of confinement has necessitated developing a multilayer protective membrane around the sample; this element is composed of 8 mm of latex and 2 mm of neoprene (Fig. 5). Such a set-up prevents the confining fluid from penetrating inside the sample; in addition, a plastic shield placed on the gauges protects them against possible

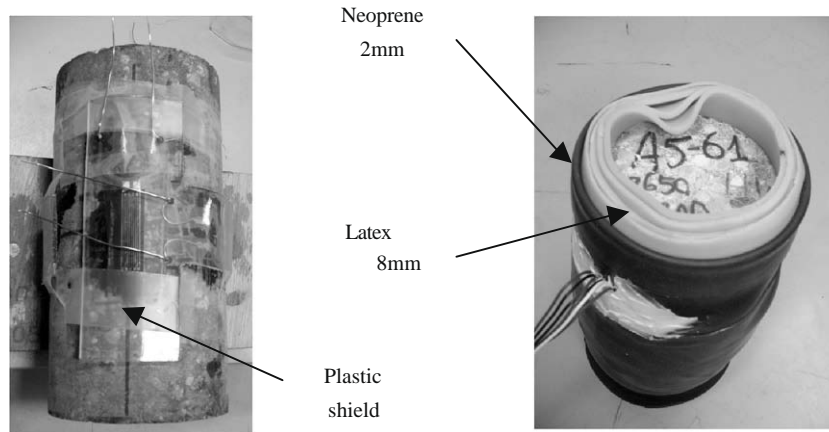


Fig. 5. Protective device placed around the sample: plastic shield (left photograph) and multilayer membrane (right).

puncture of the membrane (Vu et al., 2005; Gabet et al., 2006; Gabet et al., 2008). Fig. 5 shows the shield as well as the membrane, positioned in a sequence around the sample.

2.4. Mix proportions and concrete properties

The tested concrete displays a 28-day compressive strength of 30 MPa and a slump of 7 cm. The composition and fresh concrete properties are listed in Table 1. It should be noted that the very high-quality cement used, for purposes of better controlling material reproducibility, leads to a particularly low cement volume. Aggregate compounds containing 99% quartzite are derived from natural deposits (rolled aggregates, 99% quartzite). The maximum aggregate size (8 mm) has been chosen with respect to specimen diameter (70 mm). According to Yip and Tam (Yip and Tam, 1995), no size effect is present on the compressive strength of concrete with the selected aggregate and sample dimensions. This conclusion is assumed to be valid as well in triaxial compression.

A manufacturing procedure for the concrete samples has been established in the aim of ensuring minimal variability in mechanical properties. The concrete is cast within a parallelepiped mold by batches 13.5 l in volume. Concrete placement entails 30 s of vibration on a vibrating table. The concrete block, removed from the mold 24 h after casting, is conserved for 28 days in a saturated environment within plastic bags immersed in water, so as to insulate the concrete both physically and thermally. The block is then cored, cut and ground. All these machining stages are performed under water lubrication to avoid heating the concrete. The defect in parallelism of the two sample faces amounts to less than 0.1 mm for a 70-mm diameter.

Table 1
Compositions and mechanical properties of the studied concrete R30A7.

Concrete composition	R30A7
0.5/8 "D" gravel (kg/m ³)	1008
1800 μm "D" sand (kg/m ³)	838
CEM I 52.5 N PM ES CP2 cement (Vicat) (kg/m ³)	263
Water (kg/m ³)	169
Density (kg/m ³)	2278
<i>Mechanical properties of the concretes</i>	
Average tested strength in uniaxial compression after 28 days of aging (MPa)	28.6
Average slump measured using the Abrams cone (cm)	6.9
Volume of occluded air measured in fresh concrete (by use of an aerometer) (l/m ³)	34
Porosity accessible to water (%)	12
W/C ratio	0.64
Cement paste volume V_p (m ³ /m ³)	0.252

2.5. Concrete porosity and saturation ratio

Once the machining procedure has been completed, all samples are saturated under vacuum. Their saturated mass m_{sat} and the mass obtained from a hydrostatic weighing m_{hyd} are then measured. This weight measurement is also part of a procedure to determine concrete specimen porosity (i.e. that accessible to water) (ISO-5017, 1998). The volume of water extracted from a saturated sample after drying in an oven, at a temperature T of 50 °C and relative humidity RH of 8%, based on measurements performed on five specimens, is equal to 10.7% of the sample volume. In reference to the literature with an RH value equal to 8%, we can estimate a saturation ratio of concrete in the oven to be approximately 9.6% (Baroghel-Bouny et al., 1999), which would suggest a concrete porosity of around 12%. This value is in agreement with the concrete composition and lies very close to the mercury intrusion porosimetry measurements performed on three concrete samples 6 cm³ in volume, which would indicate a porosity value accessible to mercury of 11.5% ± 0.7%.

For each sample, the saturation ratio S_r is estimated from weight measurements as follows:

$$S_r = 1 - \frac{m_{\text{sat}} - m}{\eta(m_{\text{sat}} - m_{\text{hyd}})} \quad (1)$$

where m is the sample mass, m_{sat} the mass of the saturated sample, m_{hyd} the mass of the saturated sample obtained from a hydrostatic weighing, and η the concrete porosity, assumed to be identical for each concrete sample (i.e. $\eta = 12\%$).

2.6. Conservation of concrete samples

The samples are held in water for about 4 months, in accordance with a conservation procedure. Three kinds of samples have been tested: *dried*, *wet* and *saturated*.

After some 4 months of conservation in water, the "dried specimens" are placed in a drying oven, at a temperature T of 50 °C and relative humidity RH of 8%, for a period lasting between 3 and 6 months. Note that after 1 month of oven drying, the daily variation in sample mass does not exceed 0.1% and can thus be considered stabilized.

The "dried specimens" are then conserved in the ambient laboratory atmosphere (with T equal to about 18 °C and RH about 40%) during the instrumentation procedure, which lasts roughly 3 days prior to testing. Such a sample typically increases by around 1.4% of the water mass in its volume after 3 days. The saturation ratio of the "dried concrete" tested in this study is approximately 11%.

The “saturated specimens” are conserved in water between 6 and 10 months, after which time they are wrapped in the multi-layer membrane, just prior to the triaxial test. For such samples, strain gauge measurements are not conducted in most instances. Only the axial strain is measured from the LVDT sensor.

Lastly, the “wet specimens” are conserved in water and then a few days in the ambient laboratory atmosphere (a T value near 18 °C and 40% RH) during the instrumentation procedure.

An initially-saturated sample loses about 15% of water mass in its volume after 24 h of exposure to ambient air. In order to limit drying, the sample is kept within sealed plastic bags once no further manipulation is needed. Sample preparation with glued strain gauges on its surfaces requires at least 24 h of surface contact with ambient air. The majority of partially-saturated samples have therefore been tested with a concrete possessing a saturation ratio equal to 85%. In the remainder of this article, such samples will be referred to as *very wet*. Some so-called *wet* samples with intermediate saturation ratios have also been tested ($Sr = 42\text{--}70\%$). It should be pointed out that the conservation conditions of wet samples do not ensure a homogeneous state for the saturation ratio in a concrete sample. This is also the case, albeit to a lesser extent, for dried samples humidified by the ambient laboratory atmosphere during the instrumentation procedure. The saturation ratio of the tested sample is presented in Table 2.

Keep in mind that gluing strain gauges onto wet samples requires a specific preparation. A thin layer of glue is applied to the surfaces reserved for the gauges; this step makes it possible to isolate the gauges from the wet concrete. It then becomes necessary to obtain good gauge adhesion on the sample and effective operations during the test.

Moreover, the triaxial test at a confinement of 200 MPa on a saturated sample has been instrumented with gauges. This sample has been prepared in accordance with a specific instrumentation procedure (not described in this paper), which allows avoiding the drying phenomenon for the sample during test preparation (Vu, 2007).

Table 2

Concrete saturation ratio and confining pressure for the tests; (*) tests conducted by Gabet (Gabet et al., 2008).

Saturation ratio, Sr (%)	Confinement pressure, p (MPa)	Sample reference
Sr = 11% (dried concrete)	0	UC-11%
	50	TX50-11%
	100 (*)	TX100-11%
	200 (*)	TX200-11%
	400 (*)	TX400-11%
	500 (*)	TX500-11%
	650	TX650-11%
Sr = 42%	0	UC-42%
Sr = 50%	400	TX400-50%
Sr = 70%	200	TX200-70%
	650	TX650-70%
Sr = 85% (very wet concrete)	50	TX50-85%
	100	TX100-85%
	400	TX400-85%-a
	400	TX400-85%-b
	650	TX650-85%
Sr = 100% (saturated concrete)	0	UC-100%-a
	0	UC-100%-b
	50	TX50-100%
	100	TX100-100%
	200	TX200-100%
	400	TX400-100%
	650	TX650-100%

2.7. Age of concrete

All tested samples consist of a concrete aged between 6 and 10 months. To better quantify the effect of this parameter, we measured the evolution in concrete strength for uniaxial compression versus both conservation time and method. For concrete conserved in water, the variation in strength diminishes considerably beyond an age of 2 months. Between 6 and 10 months of age, the strength increase remains less than 1.3%. For wet samples, the rise of strength between 6 and 10 months appears to be inversely proportional to the saturation level (2.4% at $Sr = 85\%$ versus 12% at $Sr = 11\%$). However, this remains only slightly significant compared to the dispersion in results for dried concrete, i.e. approximately 7%.

For the remainder of this article, the effect of concrete age variation on results will be neglected; the concrete is considered to be 8 months old.

2.8. Loading path

In this paper, compressive stresses and contraction strains are assumed to be positive; σ_x is the principal axial stress, p the pressure inside the confining cell, σ_m the mean stress and q the principal stress difference (deviatoric stress), i.e.

$$\sigma_m = \frac{\sigma_x + 2p}{3} \quad (2)$$

$$q = \sigma_x - p \quad (3)$$

All tests have been conducted in following the same kind of loading path (Fig. 6). The triaxial compression test begins with a hydrostatic test, which consists of applying a confining pressure all around the specimen. This pressure increases at a constant stress rate of 1.67 MPa/s. Once the desired confinement has been reached, the specimen is then loaded axially at a constant displacement rate of 20 $\mu\text{m/s}$ (i.e. a strain rate of about 10^{-4} s^{-1}) while holding the confining pressure constant. Note that a maximum deviatoric stress value has not been imposed. It is a result of the test. The same path is then followed during the unloading part of the test. Uniaxial compression tests have been performed on a different laboratory press, at a strain rate of about 10^{-5} s^{-1} . A summary of the tests carried out for this study is presented in Table 2.

3. Test results

This section will display test results in terms of axial stress versus strain components. The uniaxial compression tests allow comparing our results with those from the literature regarding the effect of concrete saturation ratio on uniaxial behavior. Triaxial test results will indicate the sizable influence of saturation ratio on the behavior of heavily-confined concrete.

3.1. Uniaxial compression tests

Fig. 7 depicts the evolution in axial stress versus strain components for the uniaxial compression tests. Table 3 lists the conservation conditions and numerical values of both the Young's modulus E and Poisson's ratio identified from these tests. The curves in Fig. 7 show that concrete behavior in uniaxial compression is not considerably affected by the saturation ratio variation. It can still be observed that the Young modulus seems to marginally decrease as the concrete dries. Others uniaxial compression tests have been carried without any strain measurements (Vu, 2007). The results show that the scatter of the ultimate stress is about 7% for dried concrete and less than 1% for saturated concrete.

The strength variation (peak ultimate stress) actually proves to be the most significant. An increase in ultimate stress is observed

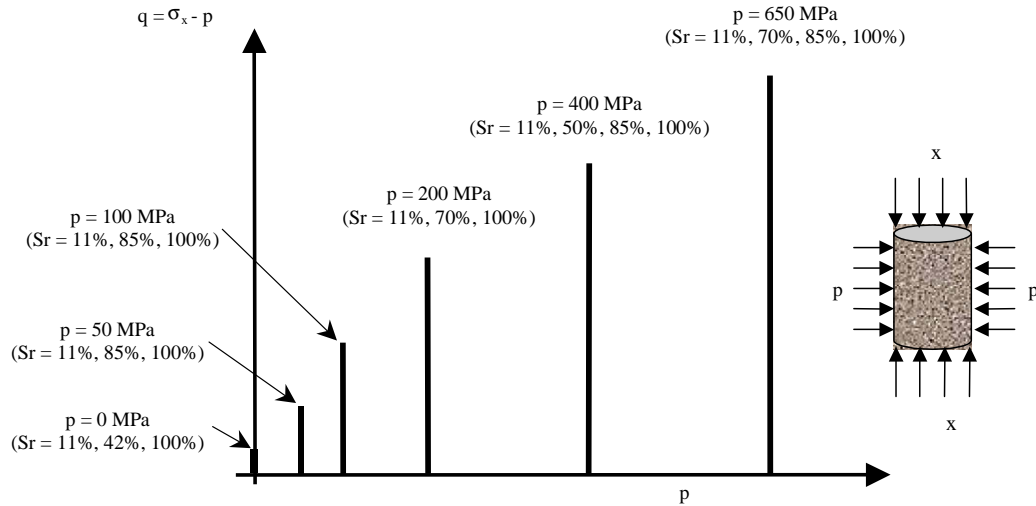


Fig. 6. Loading path for the tests: deviatoric stress q vs. confining pressure p ; σ_x : axial stress; Sr: saturation ratio of the concrete sample.

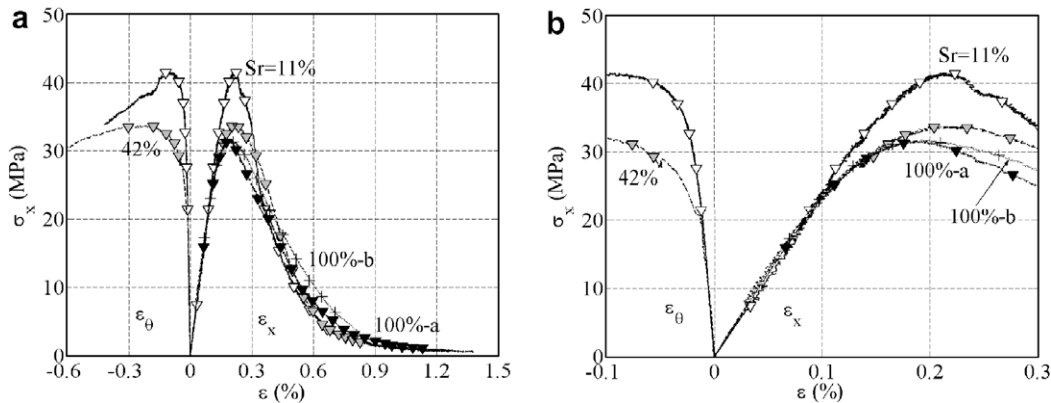


Fig. 7. Uniaxial compression tests performed on samples with various saturation ratios (Sr). (a) Axial stress σ_x vs. strain components ϵ_x and ϵ_θ . (b) Zoom of the figure in (a).

Table 3
Uniaxial compression tests – conservation conditions and concrete characteristics with various saturation ratios (Sr).

Sample reference	UC-11%	UC-42%	UC-100%-a	UC-100%-b
Saturation ratio Sr (%)	11%	42%	100%	100%
Conservation (days – d):				
- in water (water)	103 d (water) + 92 d (oven)	103 d (water) + 60 d (air)	292 d (water)	292 d (water)
- in a drying oven (oven at 50 °C)				
- in ambient air (air)				
Dimensions: D × H (cm)	7 × 14	11 × 21	7 × 14	7 × 14
Ultimate stress (σ_{max})	42 MPa	34 MPa	32 MPa	32 MPa
Young's modulus (E)	24 GPa	25 GPa	25 GPa	25 GPa
Poisson's ratio (ν)	0.13	0.16	–	–

with a decrease in saturation ratio: an increase of 6% for Sr = 42% and 31% for Sr = 11%, in comparison to the saturated sample strength. These results aptly reveal the drying effect on ultimate stress, as already recorded in the literature (Pihlajaara, 1974; Brooks and Neville, 1977; Okajima et al., 1980; Torrenti et al., 1997; Yurtdas et al., 2004a; Burlion et al., 2005).

The increase in ultimate stress of a cementitious material versus its mass loss may be explained by the effects induced through the concrete drying process before the test. Drying induces desiccation shrinkage by means of capillary depression (or capillary suction) variations (Bazant and Wittmann, 1982; Acker, 1988), disjunction pressure variations and surface energy variations (Acker, 1988; Wittmann, 1982). According to Yurtdas (Yurtdas et al., 2004a)

and Burlion (Burlion et al., 2005), capillary suction, generated during the evaporation of free water in capillary pores, can be considered as the dominant mechanism. This effect leads to a stiffening of the material, which acts like an isotropic compression of the granular skeleton, with the material exhibiting a higher strength as if it were confined.

In addition, the axial mechanical loading causes on the low permeability saturated samples an increase of interstitial pressure. This interstitial overpressure may have an amplifying effect on the propagation and opening of microcracks (Yurtdas et al., 2004a; (Burlion et al., 2005; Popovics, 1986) and leads to a decrease in strength of the saturated concrete in comparison with the dried concrete.

Furthermore, the non-uniformity of internal humidity in the concrete structure leads to creating hydrous gradients (Bazant and Wittmann, 1982; Acker, 1988; Wittmann, 1982; Bisschop et al., 2001). Shrinkage strains are indeed prevented by a structural effect: the central part dries more slowly than the surface and prevents surface shrinkage, which induces contraction and micro-cracking within the external part of the dried sample. Contraction of the external part leads to confinement over the central part, which then induces an increase in sample strength and a decrease in Young's modulus in comparison with the saturated sample.

3.2. Triaxial tests

Fig. 8 illustrates the evolution in axial stress versus strain components during triaxial tests carried out for various saturation ratios at different confining pressures. The axial strain represented has been obtained from the LVDT sensor measurement, while the circumferential strain is the average strain measured by the two diametrically-opposite gauges. In order to facilitate comparison of the curves, the scales on all four graphs are made identical.

During the hydrostatic phase of testing, it is observed that most tests follow the same stress–strain curve for a given saturation ratio, which suggests good reproducibility of concrete behavior even though the samples stem from different blocks, cast on different dates. This finding indicates on the one hand that both the concrete production procedures and sample preparation procedures are relevant. This finding shows on the other hand a low sensitivity of the confined behavior to an ensemble of parameters that may vary during the concrete making. Moreover, on most of the tests performed, the axial and circumferential strains are very close to

one another during the hydrostatic phase, which reflects that the concrete behavior is almost isotropic at these loading levels.

For confinement levels of 50 and 100 MPa, results show a concrete behavior that seems to be similar regardless of the concrete saturation ratio (see Fig. 8a, b and d). For higher confinement levels, the results on dried samples indicate that the concrete loading capacity increases significantly with confining pressure (Fig. 8a). For these tests, no stress peak can be reached prior to unloading. In contrast, tests on the very wet or saturated samples present a more ductile behavior with an axial stress threshold in plateau form regardless of the confinement pressure (Fig. 8b and d).

Fig. 8c presents the results from tests performed on samples with different intermediate saturation ratios. For a saturation ratio of 70%, the TX200-70% test has an axial stress peak, followed by slight strain softening, whereas a perfectly horizontal plateau is observed for the TX650-70% test.

The TX400-50% test seems to be fairly characteristic of wet concrete behavior (Fig. 8c); it shows a marked increase in material loading capacity with axial deformation during the early deviatoric phase, then ultimately reaches a plateau at the end of loading. This test demonstrates that under high mean stress, wet concrete behavior is similar to that of dried concrete at the beginning of loading (i.e. high strain hardening) and becomes similar to that of saturated concrete at high strain levels (i.e. horizontal plateau).

4. Volumetric behavior

In order to more accurately evaluate the effect of saturation ratio on concrete behavior, this section will present the volumetric

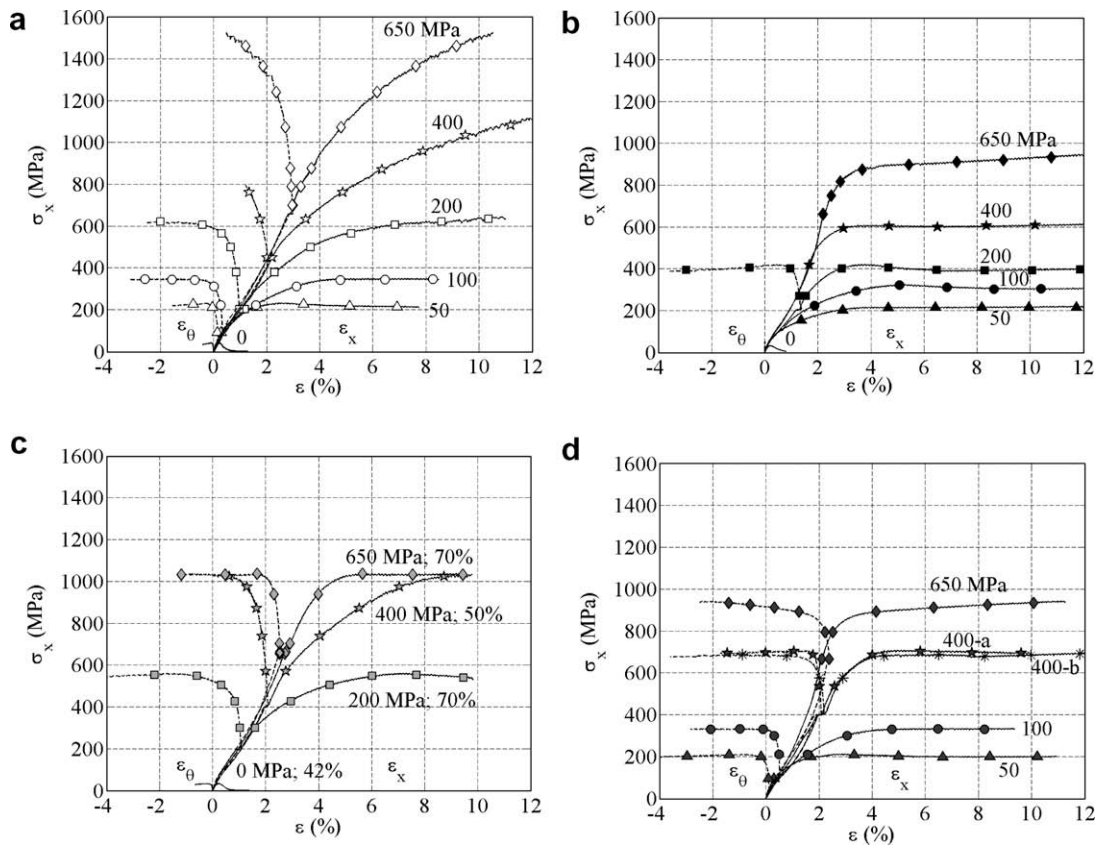


Fig. 8. Results of triaxial tests for various saturation ratios at different confining pressures p : axial stress σ_x vs. strain components ϵ_x (continuous line) and ϵ_θ (dashed line); Sr: saturation ratio; $p = 0$ MPa (no marker), 50 MPa (triangle), 100 MPa (circle), 200 MPa (square), 400 MPa (star), 650 MPa (diamond); dried concrete: white symbols; saturated concrete: black symbols; wet concrete: light grey symbols; very wet concrete: dark grey symbols; tests with confinement levels of 100, 200 and 400 MPa on dried concrete conducted by Gabet (Gabet et al., 2008). (a) Dried concrete – Sr = 11%. (b) Saturated concrete – Sr = 100%. (c) Wet concrete – Sr = 42%, 50%, 70%. (d) Very wet concrete – Sr = 85%.

behavior curves derived from both saturation ratio and confinement levels. The mean stress and volumetric strain values have all been estimated from the measurements provided in the previous section, using Eqs. (2) and (4):

$$\varepsilon_v = \varepsilon_x + 2\varepsilon_\theta \tag{4}$$

4.1. Effect of confining pressure on volumetric behavior

Fig. 9 shows the evolution in mean stress versus volumetric strain during a test at various confining pressures. The four graphs, whose scales are identical, correspond to different concrete saturation ratios. Be aware that for tests carried out without gauges (i.e. Sr = 100%, Fig. 9b), only the hydrostatic phase of the test is represented. The volumetric strain is estimated from the axial strain measurement by considering that the concrete is completely isotropic:

$$\varepsilon_v = 3\varepsilon_x \tag{5}$$

The first part of the curves in Fig. 9 corresponds to the hydrostatic loading phase. It is observed that regardless of the saturation ratio, the behavior remains linear up to a mean stress of about 40–50 MPa. This elastic phase of the concrete hydrostatic behavior is characterized by a compressibility modulus of around 11,000 MPa, with an apparently low dependence on the saturation ratio.

Beyond this linear phase, the observed gradual decrease in the tangent modulus of the concrete can be attributed to progressive damage of the cementitious matrix due to hydrostatic compression. This phase continues until reaching an inflection point at a stress level between 100 and 200 MPa, which marks the transition toward a gradual increase in tangential stiffness. This last behavioral phase may be explained by the sample volume decrease,

which in turn induces material densification and thus an increase in stiffness.

A comparison of the four graphs in Fig. 9 shows that the successive slope variations between the three phases described above seem to be more pronounced for high concrete saturation ratios.

The second part of the curves corresponds to the deviatoric phase of loading (see Fig. 9a, c and d). At the beginning of this stage, a systematic slope reduction is observed, which indicates that for a given mean stress, concrete compaction is enhanced by the presence of a deviatoric stress. This effect is more distinct when sample confinement level is small.

The final part of the curves however shows that this phenomenon winds up reversing itself. In approaching the peak stress, the concrete behavior turns to dilatancy. For samples with high saturation ratios (Sr = 70–100%), the transition point from material contraction to dilatancy is very pronounced and coincides with the peak stress (Fig. 9 c and d). Such is also the case for dried samples tested at confinement levels below 200 MPa (Fig. 9a). On the other hand, at high confinement levels with dried concrete, this transition is much less distinct. As an example, for the TX650-11% test (Fig. 9a), it is observed that the appearance of dilatancy lies well below the maximum axial stress level. Note that an absolute maximum stress has not been reached during this test.

4.2. Effect of saturation ratio on volumetric behavior

Figs. 10 and 11 display the volumetric behavior curves for various saturation ratios. Each graph corresponds to one of the tested confinements: 0 MPa (Fig. 10a), 50 MPa (Fig. 10b), 100 MPa (Fig. 10c), 200 MPa (Fig. 10d), 400 MPa (Fig. 11a), and 650 MPa (Fig. 11b and c). Figs. 10 and 11 reveal that the volumetric behavior

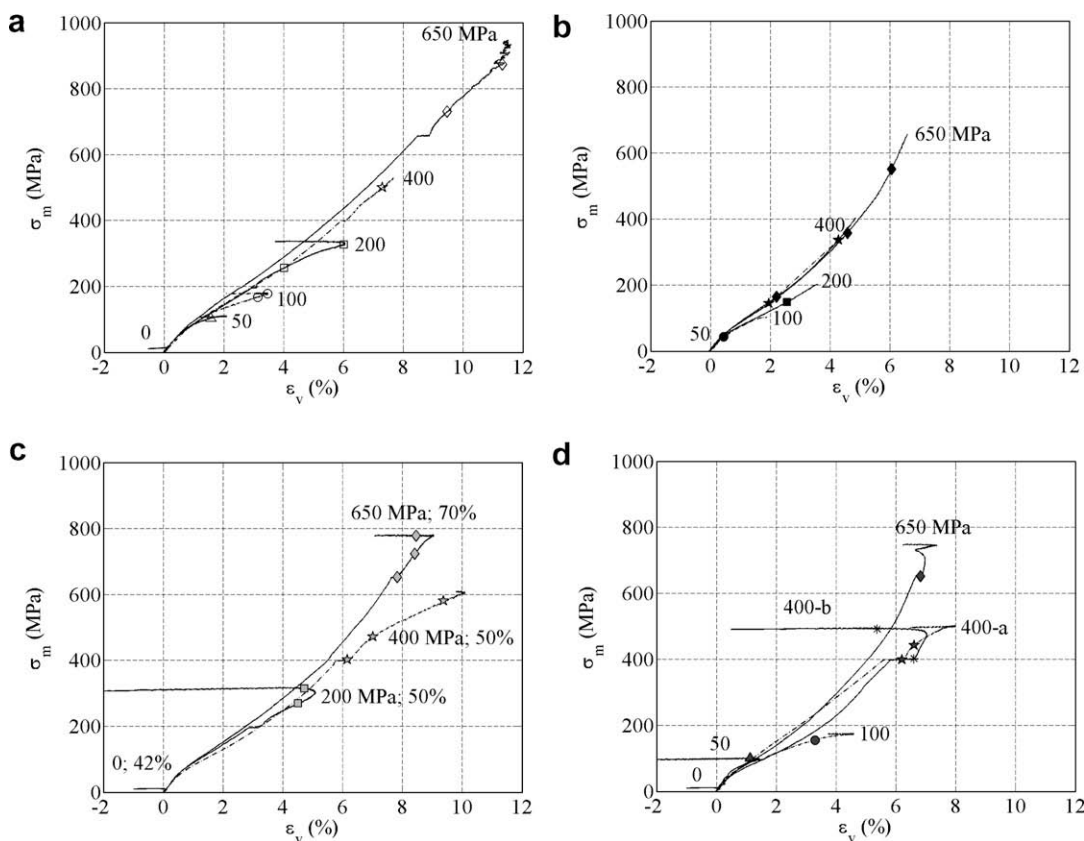


Fig. 9. Effect of confining pressure p on the concrete volumetric behavior for different saturation ratios S_r : mean stress σ_m vs. volumetric strain ε_v . (a) Dried concrete - $S_r = 11\%$. (b) Saturated concrete - $S_r = 100\%$. (c) Wet concrete - $S_r = 42\%$; 50%; 70%. (d) Very wet concrete - $S_r = 85\%$.

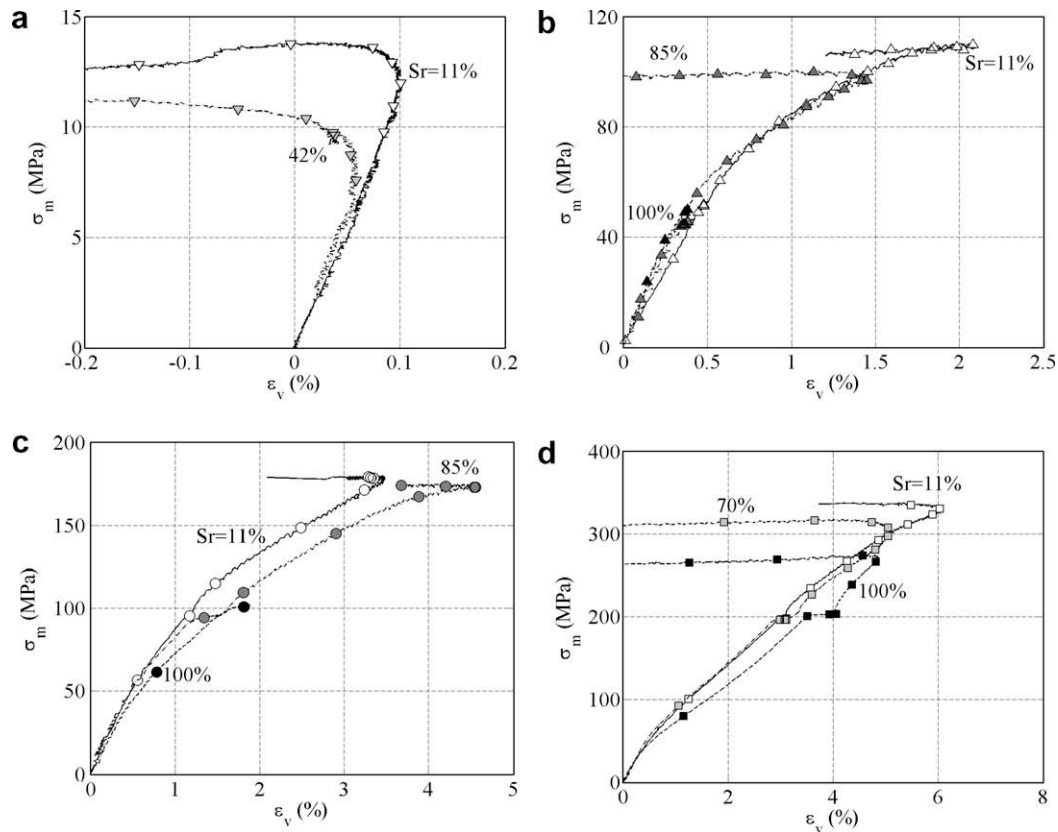


Fig. 10. Effect of saturation ratio S_r on concrete volumetric behavior for various confining pressures p . Mean stress σ_m vs. volumetric strain ϵ_v ; dried concrete: white symbols; saturated concrete: black symbols; wet concrete: light grey symbols; very wet concrete: dark grey symbols. (a) $p = 0$ MPa, (b) $p = 50$ MPa, (c) $p = 100$ MPa, (d) $p = 200$ MPa.

curves for concretes with different saturation ratios actually intersect twice.

For mean stress levels below roughly 50 MPa, Fig. 10b and c shows that the volumetric strain of wet concrete is slightly lower than that of dried concrete. This phenomenon can be explained by the microcracking caused by drying of the virgin material. The dried concrete has been conserved in a drying oven at 50 °C before the test, and its level of microcracking exceeds that of the concrete conserved in water.

For stress levels lying roughly between 50 and 300 MPa, the initial microcracking of the concrete is completely closed and no longer exerts any influence. The volumetric compressibility of wet or saturated concrete now exceeds that of dried concrete (Figs. 10d, b and c, and Fig. 11c). This phenomenon could be explained by two combined effects: the presence of water in the very wet or saturated samples causes dilatancy of the cement gel (Mills, 1960) and reduces both the cohesion forces and stiffness of the cementitious matrix in comparison with dried concrete. Furthermore, the presence of free water plays the role of lubricant between solid grains during this phase when concrete compaction is particularly intense.

Lastly, for a mean stress greater than around 300 MPa, the volumetric behavior of the very wet or saturated concrete definitely becomes stiffer than that of dried concrete (Fig. 11b, c and a). A relative difference of about 25% between the volumetric strains of dried and saturated samples at a mean stress of 650 MPa can for example be noted. For these stress levels, the volumetric strains become significant in comparison with the initial air volume of the sample. The initially very wet samples thus trend toward a degree of humidity close to saturation. The concrete that had also lost its cohesion then behaves like an undrained, saturated granular material. The pore pressure developing within the material rises

and exerts a significant impact on the measured stress, as observed in Fig. 11b.

It should moreover be pointed out that for most samples with differing intermediate saturation ratios ($S_r = 50$ – 70%), the behavior curve lies between very wet concrete and dried concrete (Fig. 11).

5. Deviatoric behavior

In order to more accurately evaluate the saturation ratio effect on concrete behavior, this section will present the deviatoric behavior curves as a function of both saturation ratio and confinement level. The deviatoric stress has been estimated from measurements according to Eq. (3).

5.1. Effect of confining pressure on deviatoric behavior

Fig. 12 shows the evolution in deviatoric stress versus deformation components during a test using various confinement pressures. Only the deviatoric testing phase has been depicted. Fig. 12a corresponds to the tests conducted on dried concrete, while 12b reflects those carried out on saturated concrete. The two graphs contain identical scales; Fig. 12c and d provides a close-up of the same graphs.

Fig. 12a indicates that the deviatoric behavior of dried concrete is highly dependent upon confining pressure. As strain rises ($\epsilon_x > 2\%$), the deviatoric level attained increases sharply with confining pressure. Fig. 12b however demonstrates that this effect is not significant for saturated samples. At high strain levels, the deviatoric behavior of saturated concrete seems to be independent of confining pressure.

This phenomenon is explained by the cohesion loss of the cementitious matrix under high mean stress. Because of this loss,

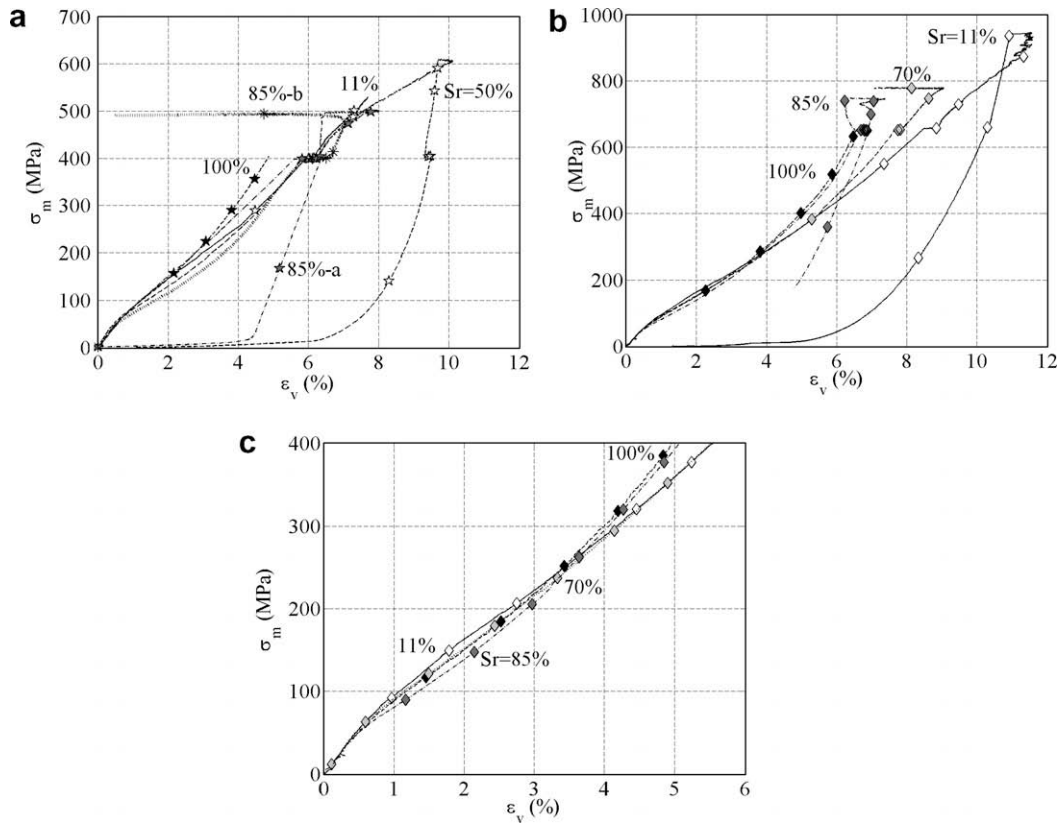


Fig. 11. Effect of saturation ratio S_r on concrete volumetric behavior for various confining pressures p : mean stress σ_m vs. volumetric strain ϵ_v ; dried concrete: white symbols; saturated concrete: black symbols; wet concrete: light grey symbols; very wet concrete: dark grey symbols (a) $p = 400$ MPa, (b) $p = 650$ MPa, (c) $p = 650$ MPa (close-up of Fig. 11b).

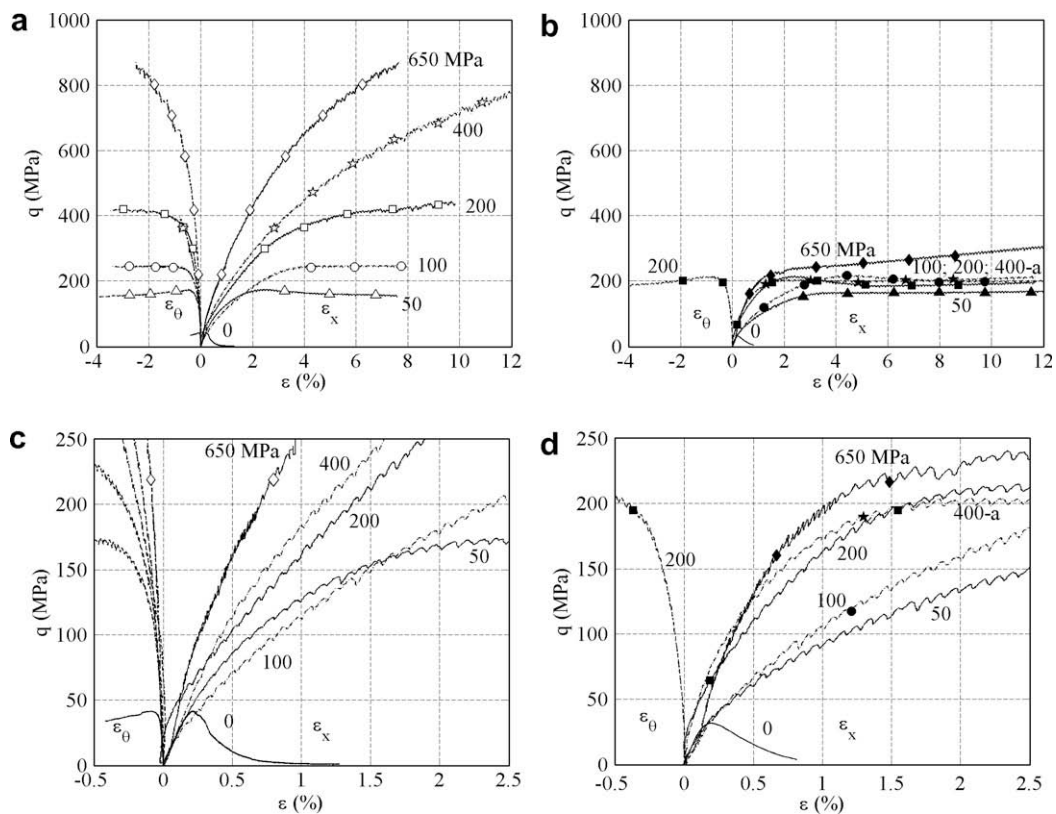


Fig. 12. Effect of confining pressure on the deviatoric behavior of dried and saturated concretes: Deviatoric stress q vs. strain components ϵ_x and ϵ_θ ; p : confining pressure; S_r : saturation ratio of the sample; dried concrete: white symbols; saturated concrete: black symbols. (a) Dried concrete $S_r = 11\%$. (b) Saturated concrete $S_r = 100\%$. (c) Dried concrete $S_r = 11\%$ (close-up of Fig. 12a). (d) Saturated concrete $S_r = 100\%$ (close-up of Fig. 12b).

the concrete behaves like an undrained, non-cohesive and saturated granular stacking sequence, whose volume decrease generates an increase in pore pressure. This phenomenon becomes more acute with increases in confinement, strain level and saturation ratio.

Note that the behavior observed for saturated concrete under high confinement is similar to that of soils for which the maximum deviatoric stress on saturated samples remains constant regardless of confining pressure.

Fig. 12c and d provides a more accurate view of the concrete deviatoric behavior at low confinement levels. These figures show that the evolution in initial tangential stiffness of concrete with respect to confinement is similar for dried and saturated samples. Table 4 lists the numerical values of the concrete initial tangent modulus for various confinements for both dried and saturated samples. For confinement levels above 100 MPa, the axial tangent stiffness of samples increases with confinement. On the other hand, the opposite effect is found for confinement levels less than 100 MPa: the tangent stiffness of concrete decreases as confinement rises.

This phenomenon is consistent with the previously-observed material hydrostatic response, which indicates material softening up to a mean stress level of about 150 MPa, followed by stiffening (see Figs. 8 and 9). Moreover, it is explained by both the gradual damage to the cementitious matrix, which predominates at low confinement, and material densification causing stiffening under high confinement.

5.2. Effect of saturation ratio on deviatoric behavior

Fig. 13 shows the deviatoric behavior curves for various saturation ratios. Each graph corresponds to a given confinement level: 50 MPa (Fig. 13a), 100 MPa (Fig. 13b), 200 MPa (13c), 400 MPa (13d) and 650 MPa (13e).

Fig. 13a and b reveals that at low confining pressure, the concrete deviatoric behavior is slightly influenced by the saturation ratio. The behavior curves of dried concrete overlap with those of very wet concrete up to a point slightly below the peak stress. It is then noted that the peak stress value rises as the concrete dries. This difference in peak stress values is very low for a 50-MPa confinement and increases with confining pressure; however, it still remains moderate even for a confinement of 100 MPa.

These findings are consistent with the evolution in concrete volumetric behavior presented above. At a low mean stress level (i.e. $\sigma_m \leq 150$ MPa), collapse of the cementitious matrix remains limited. The deviatoric behavior of samples is governed by the still cohesive character of the material, which explains the slight influence of the saturation ratio.

For higher confining pressure levels, Fig. 13c, d and e indicates that the tangential stiffness of concrete at the beginning of the axial loading phase is only very slightly dependent on the saturation ratio. The deviatoric behavior curves of saturated concrete lie very close to those for dried concrete up to a deviatoric stress level of

approx. 200 MPa. This value constitutes a threshold for the saturated samples regardless of confinement level. The resistance capacity of the dried samples is clearly higher. As such, no peak deviatoric stress is reached in the tests conducted on dried concrete at these high confinements.

These results may be explained by the cohesion loss of the cementitious matrix, which provides the concrete with a behavior of the non-cohesive granular material type. The increase in dried concrete shear strength with confining pressure is thus explained by the friction existing between stacking grains. Limitation of the same strength observed for saturated concrete is probably due to pore pressure, which develops similarly to what is found in undrained soils.

For intermediate saturation ratios, Fig. 13b, c, d and e demonstrates that the deviatoric behavior of concrete lies between the dried and saturated limit cases. For a given confinement, the peak deviatoric stress seems, in particular, to be directly correlated to the concrete saturation ratio. The peak stress level rises as the concrete dries. This last point will be developed in greater detail in the following section.

6. Limit states

During the experimental characterization of material behavior, various criteria may be used to identify a material's limit state curve. The most commonly used criterion has been defined as the stress state associated with the maximum deviatoric stress that the material can support (i.e. the stress limit state). For geomaterials exhibiting dilating behavior upon fracture, this stress limit state often lies close to the stress state associated with the transition point from material contraction to dilatancy. This state corresponds to the maximum volumetric strain state, in terms of contraction, that the material can reach (i.e. the strain limit state). Figs. 14 and 15 show, within the (σ_m, q) plane, the limit states in both stress and strain identified from the results presented earlier. Fig. 14 focuses on the tests conducted on dried or slightly wet concrete, while Fig. 15 corresponds to tests carried out on very wet or saturated concrete.

Fig. 14 indicates that for mean stress levels below 200 MPa, the limit states in both strain and stress nearly overlap with one another. For mean stress levels above 300 MPa, the difference between these states becomes significant and tends to heighten with an increase in confinement. The stress limit state curve seems just about linear within the (σ_m, q) plane, while the strain limit state curve displays slight curvature. Note that the capacity of this experimental device does not allow a precise identification of the stress limit state of dried concrete for confining pressures above 200 MPa. Beyond this confinement, the strain level associated with the stress exceeds the strain gauge validity range ($\epsilon_x > 18\%$). The stress limit state curve therefore has not been accurately determined. The maximum stress state reached prior to unloading simply provides a lower bound.

From a physical standpoint, the quasi-linear nature of the limit state curve reinforces the notion that concrete under high confinement behaves like a slightly cohesive granular stacking sequence governed by friction phenomena.

Fig. 15 presents the stress and strain limit states for the wet or saturated samples ($S_r = 70\text{--}100\%$). This figure indicates that for tests carried out at high confinement on a very wet concrete, the difference between the stress and strain limit states turns out to be very small; it only proves significant for the TX200-70% test, which corresponds to the lowest confinement value of the saturation ratio.

Most saturated samples have been tested without gauges; for these tests, the volumetric strain cannot be determined during the deviatoric phase of the test. Given the observations forwarded

Table 4
Evolution of the initial axial tangent modulus of concrete with confinement.

Confining pressure (MPa)	Initial axial tangent modulus (GPa)	
	Dried concrete ($S_r = 11\%$)	Saturated concrete ($S_r = 100\%$)
0	24.0	32.0
50	21.5	17.5
100	17.5	15.0
200	21.9	22.3
400	25.1	35.2
650	50.0	42.1

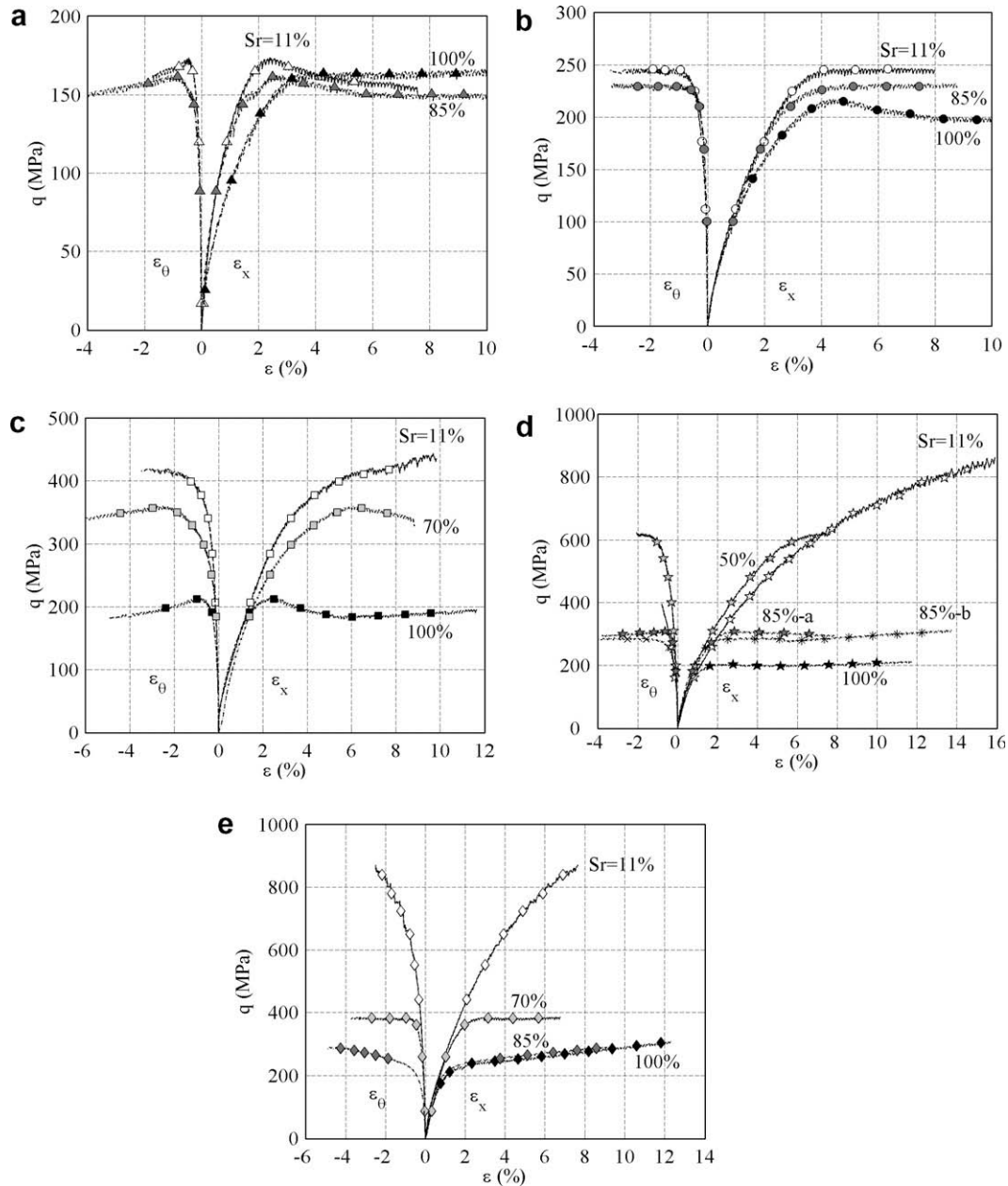


Fig. 13. Effect of saturation ratio on the concrete deviatoric behavior for various confining pressures p : axial stress q vs. strain components ε_x and ε_θ ; dried concrete: white symbols; saturated concrete: black symbols; wet concrete: light grey symbols; very wet concrete: dark grey symbols (a) $p = 50$ MPa. (b) $p = 100$ MPa. (c) $p = 200$ MPa. (d) $p = 400$ MPa. (e) $p = 650$ MPa.

in Fig. 15 however, it may be assumed that the stress and strain limit states coincide for these tests, whose deviatoric stress threshold is easily identifiable (see Fig. 12b and d). Under this hypothesis, the strain limit state corresponding to the material transition point from contraction to dilatancy can be determined and compared for all tested samples regardless of the saturation ratio and confinement level.

Fig. 16 shows strain limit states in the (σ_m, q) plane for all tested samples. This figure reveals that the deviatoric level associated with the material transition point from contraction to dilatancy increases rapidly and almost linearly with the mean stress for dried concrete. Dilatancy of the dried samples under high confinement is explained by a rearrangement of the granular stacking sequence composing the concrete. The shear stresses generate aggregate movement in the matrix, which initially serves to stimulate compaction. Once the maximum compaction level has been reached,

the sample expands (Gabet et al., 2008). The failure surface of concrete has been described in various ways for numerical modeling purpose. In most common models, one can find three kinds of meridian cross section of the failure surface: linear (Mohr-Coulomb, Drucker and Prager, 1952; Williams and Warnke, 1974), parabolic (Mises-Schleicher, 1926; Nadai, 1950; Krieg, 1972; Swenson and Taylor, 1983) or power law (Kang and Willam, 1999). To compare these models with the results, a comparison between the limit states of the dried concrete and these three kinds of failure surfaces is shown in a log-log plot on Fig. 17. The best fitting parameters and the discrepancy with the measurements are display on Table 5. For mean stresses higher than 100 MPa, the limit state curve is almost linear and the three kinds of model are close to the results. However, the power law gives the best fitting with a mean error equal to 3%. For lower mean stresses the linear or parabolic criterions leads to an overestimation of the concrete strength. These cri-

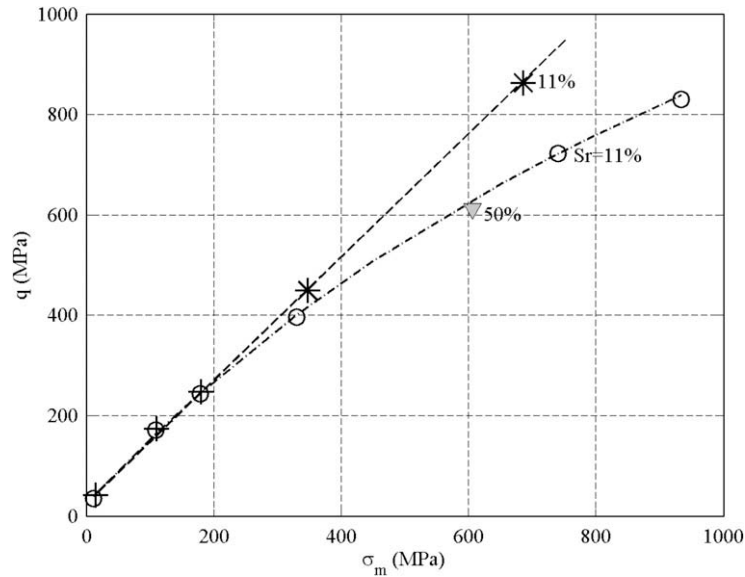


Fig. 14. Limit states of the slightly wet or dried concrete (Sr = 50%; 11%): deviatoric stress q vs. mean stress σ_m ; \circ = strain limit state (Sr = 11%); $+$ = stress limit state (Sr = 11%); $*$ = limit state attained (Sr = 11%); light grey triangle-down symbol = strain limit state (Sr = 50%); dash-dot line = strain limit state curve (Sr = 11%); dashed line = shape of the stress limit state curve (Sr = 11%).

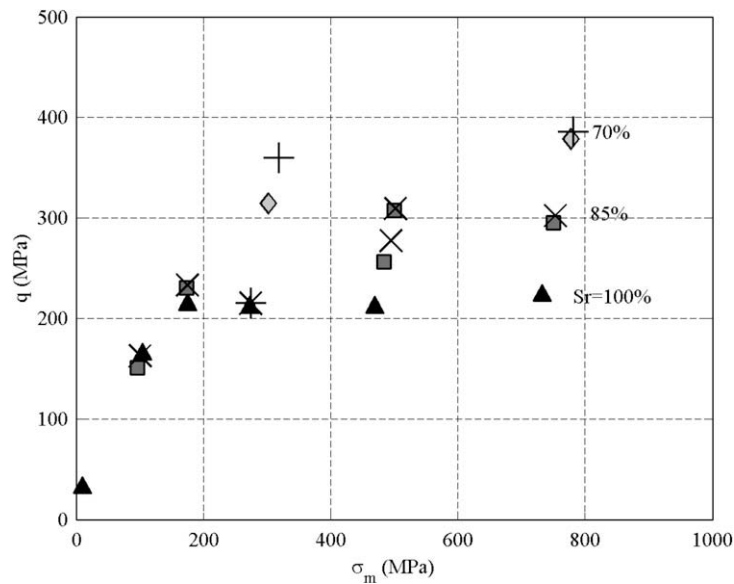


Fig. 15. Limit states of the very wet or saturated concrete (Sr = 70%; 100%): deviatoric stress q vs. mean stress σ_m ; light grey diamond symbols = strain limit state (Sr = 70%); $+$ = stress limit state (Sr = 70%); dark grey square symbols = strain limit state (Sr = 85%); \times = stress limit state (Sr = 85%); \blacktriangle = strain limit state (Sr = 100%); $*$ = stress limit state (Sr = 100%).

terions are not able to fit the simple compression strength whereas the power law is close to measurements in the all range. One can notice that the identified exponent of the power law ($c = 0.758$) is very close to the one proposed by Kang ($c = 0.77$, Kang and Willam, 1999) from various experimental results taken from literature.

At a low level of mean stress (below 150 MPa), it is found that the limit states of the dried, wet and saturated samples all lie very close to one another (Fig. 16). This result should come as no surprise since at such stress levels, concrete behavior is governed by a still cohesive character. The contraction–dilatancy transition is associated with the opening of microcracks in the material structure during gradual damage to the cementitious matrix (Mazars, 1984). The presence of water in the sample does not exert therefore a very significant effect on the limit state.

Conversely, the above figure shows that for higher confinement levels, the effect of water becomes predominant. The increase in peak deviatoric stress with respect to mean stress remains very low for the saturated samples. The peak deviatoric stress is just 230 MPa for a confinement of 650 MPa when the sample is saturated. This phenomenon is likely explained by a pore pressure effect similar to that observed for an undrained granular material. Moreover, it can be observed from Fig. 16 that the limit states of wet samples under high confinement lie between those of dried and saturated samples, i.e.: $q = 300$ MPa for Sr = 85%; $q = 400$ MPa for Sr = 70%; and $q = 600$ MPa for Sr = 50%. The limit state curve would thus seem to vary with the concrete saturation ratio.

Eventually, three types of situations can be schematically distinguished for wet concrete:

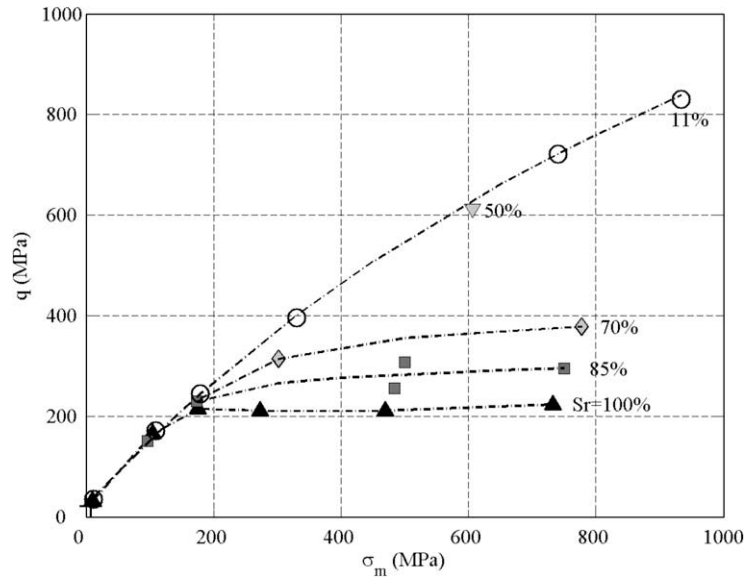


Fig. 16. Strain limit state of the concrete vs. its saturation ratio Sr: deviatoric stress q vs. mean stress σ_m ; o = dried concrete; $+$ = wet concrete (Sr = 42%); light grey triangle-down symbol = wet concrete (Sr = 50%); light grey diamond symbols = wet concrete (Sr = 70%); dark grey square symbols = very wet concrete; \blacktriangle = saturated concrete; dash-dot lines = strain limit state curves for various saturation ratios.

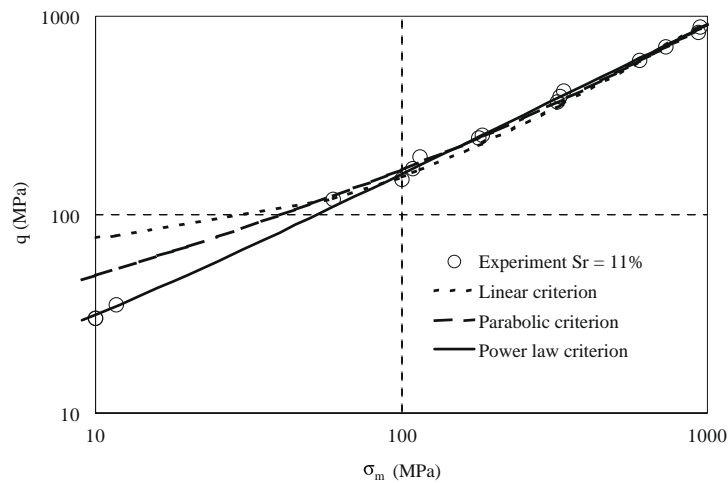


Fig. 17. Comparison between the limit states of the dried concrete and the most common concrete criterions; experiment on dried concrete (o); linear criterion $q = b + c\sigma_m$ (dot line); parabolic criterion $q = (a + b\sigma_m + c\sigma_m^2)^{1/2}$ (dash line); power law criterion $q = a(b + \sigma_m)^c$ (full line).

Table 5
Identified parameters from common criterion and discrepancy between the measurements and the fitting.

	Linear ($q = b + c\sigma_m$)	Parabolic ($q = (a + b\sigma_m + c\sigma_m^2)^{1/2}$)	Power law ($q = a(b + \sigma_m)^c$)
a (MPa ²)	-	177	4.81
b (MPa)	68.7	221	1.82
c	0.868	0.621	0.758
Mean error	32%	14%	3%
Mean error*	6%	4%	3%
Mean error*	14%	12%	9%

* Without simple compression tests.

- At a low level of mean stress, as long as a concrete is retaining its cohesive character, the wet concrete limit state is close to that of dry concrete (see Fig. 18, Zone I).
- At the other end, when the mean stress is high and the sample is very wet, a threshold exists beyond which the air-porosity of concrete is completely closed, the concrete being then fully saturated. This threshold lies at a mean stress level that is the

higher as the concrete is more dry. Above this threshold, the peak deviatoric stress increases slightly regardless of confinement level, as is the case for saturated samples (Fig. 18, Zone II).

- Between these two extreme situations, for intermediate mean stress levels, since the free air volume of the sample has not been completely eliminated, the contraction–dilatancy transition threshold for the sample corresponds to the maximum compaction of the granular stacking sequence constituting the concrete. In this intermediate situation, water plays the role of lubricant within the sample and thus reduces the shear strength capacity of wet concrete, in comparison with that of dried concrete.

7. Conclusion

The context of this study pertains to the identification of concrete behavior under extreme loadings. In order to reproduce high levels of stress with well-controlled loading paths, static tests have been conducted on concrete samples using a very large capacity triaxial press. The test results presented in this article more specif-

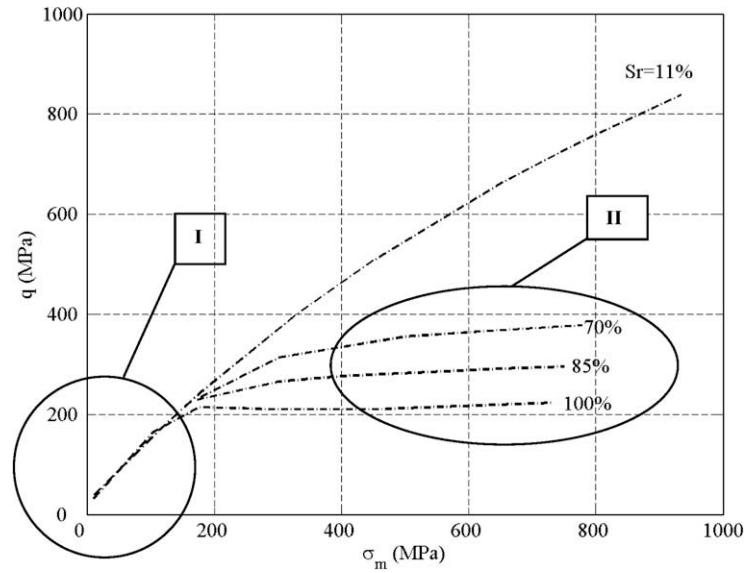


Fig. 18. Idealization of the strain limit state for wet concrete: Zone I = limit state of the “dried concrete” type; Zone II = limit state of the “saturated concrete” type; dash-dot lines = strain limit state curves for various concrete saturation ratios.

ically concern the saturation ratio effect on concrete behavior under high confinement. Triaxial tests have thus been carried out on ordinary concrete samples for saturation ratios varying from 11% (dried concrete) to 100% (saturated concrete) and for confining pressure levels between 50 and 650 MPa.

An analysis of these tests shows that the behavior of an ordinary concrete is only slightly dependent on the saturation ratio at low confining pressures. When the cementitious matrix retains a portion of its cohesion, the presence of free water in the concrete generates measurable material stiffness and strength variations, which nonetheless remain low.

In contrast, under high mean stress, the saturation ratio of concrete takes on major importance:

- The hydrostatic behavior of very wet or saturated concrete clearly becomes stiffer than that of dried concrete.
- The shear strength of very wet or saturated concrete seems limited to a maximum value independent of confining pressure, while the shear strength of dried concrete increases almost linearly with confining pressure.
- The limit shear strength value is directly correlated with the concrete saturation ratio. The concrete strength under high confinement rises as the concrete dries.

The three previous observations can be explained by a combination of two phenomena. On the one hand, the loss of cohesion in the cementitious matrix due to high confinement provides the concrete with a behavior of the non-cohesive granular material type. The dried concrete shear strength increases nearly linearly with confining pressure, and this is explained by the friction existing between stacking grains. On the other hand, the high level of volumetric strains in comparison with the sample’s initial air volume serves to trend sample humidity closer to saturation. Concrete under high confinement then behaves as an undrained, saturated granular material. The pore pressure developing in the material becomes sizable and increases the volumetric stiffness of the concrete while limiting its shear strength.

In conclusion, under high confinement, the presence of free water within the concrete significantly limits its shear resistance. For a confining pressure of 650 MPa, the shear strength of dried concrete is divided by a factor of 4 when the concrete is saturated, dropping from 900 MPa to just 230 MPa. From an application

standpoint, these results highlight the advantages derived by reducing the saturation ratio of concrete structures for the purpose of raising their strength capacity to resist extreme loadings.

The experimental device used for this study did not allow performing either drained tests or pore pressure measurements. The development of such measurements for a future study appears difficult to implement yet would allow confirming the hypotheses generated in this article. For the time being, this study is limited to ordinary concretes. In the future, it will be necessary to evaluate the effect of concrete porosity on the validity of results. More specifically, do the above conclusions remain valid for very low porosity and/or high performance concretes?

8. Symbols and conventions

Definition of variables:

$\epsilon_x, \epsilon_\theta$	axial, circumferential strain
$\epsilon_v = \epsilon_x + 2\epsilon_\theta$	volumetric strain
p	confining pressure
σ_x	axial stress
$\sigma_m = \frac{\sigma_x + 2p}{3}$	mean stress
$q = \sigma_x - p$	deviatoric stress (deviator)
V_{air}	free air volume of the wet concrete sample
Sr	concrete saturation ratio
$Sr = 1 - \frac{m_{sat} - m}{\eta(m_{sat} - m_{hyd})}$	
m	sample mass
m_{sat}	mass of the saturated sample
m_{hyd}	mass of the saturated sample from hydrostatic weighing
η	concrete porosity accessible to water

Designation of the concretes:

- Saturated concrete – Sr = 100%
- Very wet concrete – Sr = 85%
- Wet concrete – Sr = 70%, 50%, 42%
- Dried concrete – Sr = 11%

Sign conventions:

- $\sigma \geq 0$ during compression
- $\epsilon \geq 0$ during contraction

Abbreviations:

TX50-11% triaxial test, conducted at 50 MPa, of confining pressure on a concrete sample displaying a saturation ratio of 11% ($p = 50$ MPa, $Sr = 11\%$)

UC-100% uniaxial compression test conducted on a saturated concrete sample ($p = 0$ MPa, $S_r = 100\%$)

Acknowledgments

The GIGA press has been installed in the 3S-R laboratory within the framework of a cooperative agreement signed with France's *Délégation Générale pour l'Armement* (CEG, DGA, French Ministry of Defense, General Delegation for Ordnance). This research has been performed thanks to financial support received from the "Centre d'Etudes de Gramat" (CEG, DGA).

References

- Acker, P., 1988. Comportement mécanique du béton: apport de l'approche physico-chimique. PhD thesis of Ecole Nationale des Ponts et des Chaussées, Paris, Rapport de Recherche LPC n°152 (in French).
- Akers, S.A., Phillips B.R., 2004. Concrete modelled as an inhomogeneous material: numerical simulations of contact detonation charges. In: Proceedings of the 18th International Symposium on the Military Aspects of Blast and Shock, Oberjettenberg, Germany.
- Bailly, P., Tombini, C., Le Vu, O., 1996. Modélisation de géomatériaux sous sollicitations dynamiques élevées. I: Un tir de pénétration sur cible en béton. Colloque du réseau GEO, Aussois, 2–6 December, France (in French).
- Baroghel-Bouny, V., Mainguy, M., Lassabatere, T., Coussy, O., 1999. Characterization and identification of equilibrium and transfer moisture properties for ordinary and high-performance cementitious materials. *Cement and Concrete Research* 29, 225–238.
- Bazant, Z.P., Wittmann, F.H., 1982. In: *Creep and Shrinkage in Concrete Structures*. J. Wiley and Sons.
- Bazant, Z.P., Bishop, F.C., Chang, T.P., 1986. Confined compression tests of cement paste and concrete up to 300 Ksi. *ACI Journal* 33, 553–560.
- Bischoff, P.H., Perry, S.H., 1991. Compressive behavior of concrete at high strain rates. *Materials and Structures* 24, 425–450.
- Bisschop, J., Pel, L., van Mier, J.G.M., 2001. Effect of aggregate size and paste volume on drying shrinkage microcracking in cement-based composites. In: Ulm, F.-J., Baeant, Z.P., Wittmann, F.H. (Eds.), *Creep, Shrinkage & Durability Mechanics of Concrete and other Quasi-Brittle Materials*. Elsevier, pp. 75–80.
- Brooks, J.J., Neville, A.M., 1977. Comparison of creep, elasticity, and strength of concrete in tension and in compression. *Magazine of Concrete Research* 29, 131–141.
- Burlion, N., Gary, G., Gating, F., 1998. Comportement expérimental en compaction statique et dynamique du microbéton MB50. In the scientific report "Comportement des ouvrages en dynamique rapide, comportement dynamique du béton", project leader Bailly P (in French).
- Burlion, N., Pijaudier-Cabot, G., Dahan, N., 2001. Experimental analysis of compaction of concrete and mortar. *International Journal for Numerical and Analytical Methods in Geomechanics* 25, 1467–1486.
- Buzaud, E., 1998. Performances mécaniques et balistiques du microbéton MB50, in the scientific report "Comportement des ouvrages en dynamique rapide, comportement dynamique du béton", project leader Bailly P (in French).
- Burlion, N., Bourgeois, F., Shao, J.-F., 2005. Effects of desiccation on mechanical behavior of concrete. *Cement and Concrete Composites* 27, 367–379.
- Drucker, D.C., Prager, W., 1952. Soil mechanics and plastic analysis on limit design. *Quarterly of Applied Mathematics* 10 (2), 157–165.
- Forquin, P., Arias, A., Zaera, R., 2007. An experimental method of measuring the confined compression strength of geomaterials. *International Journal of Solids and Structures* 44, 4291–4317.
- Gabet, T., Vu, X.H., Malécot, Y., Daudeville, L., 2006. A new experimental technique for the analysis of concrete under high triaxial loading. *Journal de Physique IV* 134, 635–640.
- Gabet, T., Malécot, Y., Daudeville, L., 2008. Triaxial behavior of concrete under high stresses : Influence of the loading path on compaction and limit states. *Cement and Concrete Research* 38 (3), 403–412.
- Hild, F., Denoual, C., Forquin, P., Brajer, X., 2003. On the probabilistic-deterministic transition involved in a fragmentation process of brittle materials strains. *Computers & Structures* 81 (12), 1241–1254.
- Hopkinson, B., 1914. A method of measuring the pressure in the deformation of high explosives or by the impact of bullets. *Philosophic Transactions of the Royal Society A213*, 437–452.
- Imran, I., Pantazopoulou, S.J., 1996. Experimental study of plain concrete under triaxial stress. *ACI Material Journal* 93 (6), 589–601.
- ISO-5017, 1998. International Organization for Standardization (ISO) Catalogue, Dense shaped refractory products – Determination of bulk density, apparent porosity and true porosity.
- Jiang, L.H., Huang, D.H., Xie, N.X., 1991. Behavior of concrete under triaxial compressive–compressive–tensile stresses. *ACI Material Journal* 88 (2), 181–185.
- Kang, H.D., Willam, K., 1999. Localization characteristics of triaxial concrete model. *ASCE Journal of Engineering Mechanics* 125, 941–950.
- Kupfer, H.B., Gerstle, K.H., 1973. Behavior of Concrete under Biaxial Stresses. *Journal of the Engineering Mechanics, Division* 99 (4), 853–866.
- Krieg, R., 1972. A simple constitutive description for soils and crushable foams. Report SC-DR-72-0883, Sandia National Laboratories, Albuquerque. 46, pp. 94–168.
- Le Vu, O., Bailly, P., Tombini, C., Lalle, P., Courchinoux, C., 1996. Modélisation de géomatériaux sous sollicitations dynamiques élevées. II: Equation d'état du béton, Colloque du réseau GEO, Aussois 2–6 décembre, 1996, France (in French).
- Li, H., Pugh, D., 1970. *Mechanical Behavior of Materials Under Pressure*. Elsevier, Amsterdam.
- Mazars, J., 1984. Application de la mécanique de l'endommagement au comportement non-linéaire et à la rupture du béton de structure. Thèse d'état de l'Université Paris VI, France (in French).
- Mills, R.H., 1960. Strength-maturity relationship for concrete which is allowed to dry, RILEM International Symposium on Concrete and Reinforced Concrete in Hot Countries (Haifa). In: Neville, A.M. (Ed.), *Properties of Concrete*, fourth ed., Pearson Prentice Hall, 1995, pp. 601–602.
- Nadai, A., 1950. *Theory of Flow and Fracture of Solids*, vol. 1. McGraw-Hill, New York.
- Okajima, T., Ishikawa, T., Ichise, K., 1980. Moisture effect on the mechanical properties of cement mortar. *Transactions of the Japan Concrete Institute* 2, 125–132.
- Pihlajavaara, S.E., 1974. A review of some of the main results of a research on the ageing phenomena of concrete, effect of moisture conditions on strength, shrinkage and creep of mature concrete. *Cement and Concrete Research* 4, 761–771.
- Popovics, S., 1986. Effect of curing method and moisture condition on compressive strength of concrete. *ACI Journal* 83 (4), 650–657.
- Rossi, P., Van Mier, J.G.M., Toutlemonde, F., Le Maou, F., Boulay, C., 1994. Effect of loading rate on the strength of concrete subjected to uniaxial tension. *Materials and Structures* 27 (5), 260–264.
- Sfer, D., Carol, I., Gettu, R., Etsé, G., 2002. Study of the behavior of concrete under triaxial compression. *Journal of Engineering Mechanics* 128 (2), 156–163.
- Schleicher, F., 1926. Der Spannungszustand an der Fließgrenze (Plastizitätsbedingung). *Zeitschrift für angewandte Mathematik und Mechanik* 6, 199–216. 45 (in German).
- Schmidt, J.M., 2003. High pressure and high strain rate behavior of cementitious materials: experiments and elastic/viscoplastic modeling. Doctoral Dissertation. University of Florida, USA.
- Swenson, D.V., Taylor, L.M., 1983. A finite element model for the analysis of tailored pulse simulation of boreholes. *International Journal for Numerical and Analytical Methods in Geomechanics* 7 (4), 469–484.
- Taliercio, A., Berra, M., Pandolfi, A., 1999. Effect of high-intensity sustained triaxial stresses on the mechanical properties of plain concrete. *Magazine of Concrete Research* 51 (6), 437–447.
- Thiot, 2004. Thiot Ingénierie, la Croix Blanche, 46130 Saint Michel Loubejou, France.
- Torrenti, J.M., Granger, L., Diruy, M., Genin, P., 1997. Modélisation du retrait du béton en ambiance variable. *Revue Française de Génie Civil* 1 (4), 687–698 (in French).
- Toutlemonde, F., 1995. Résistance au choc des structures en béton : du comportement du matériau au calcul des ouvrages. Doctoral Dissertation, ENPC (in French).
- Van Mier, J.G.M., 2007. Multi-scale interaction potentials (F-r) for describing fracture of brittle disordered materials like cement and concrete. *International Journal of Fracture* 143 (1), 41–78.
- Vu, X.H., Gabet, T., Malecot, Y., Daudeville, L., 2005. Experimental analysis of concrete behavior under severe triaxial loading. In The 2005 Joint ASCE/ASME/SES Conference on Mechanics and Materials, McMat 2005 Mechanics and Materials Conference, Baton Rouge, Louisiana, June 1–3, 2005.
- Vu, X.H., 2007. Caractérisation expérimentale du béton sous fort confinement : influences du degré de saturation et du rapport eau/ciment. Doctoral dissertation, Université Grenoble I (in French).
- Wang, C.-Z., Guo, Z.-H., Zhang, X.-Q., 1987. Experimental investigation of biaxial and triaxial compressive concrete strength. *ACI Material Journal* 84, 92–100.
- Warren, T., Fossum, A., Frew, D., 2004. Experimental investigation of size effect in concrete fracture under multiaxial compression into low-strength (23 MPa) concrete: target characterization and simulations. *International Journal of Impact Engineering* 30, 477–503.
- Williams, K.J., Warnke, E.P., 1974. Constitutive model for the triaxial behavior of concrete. International Association of Bridge and Structural Engineers Seminar on Concrete Structures Subjected to Triaxial Stresses, Paper III-1. Bergamo.
- William, E.M., Akers, S.E., Reed, P.A., 2005. Constitutive models for the triaxial behavior of concrete. Report n°ERDC/GSL TR-05-16, Geotechnical and Structures Laboratory, U.S. Army.
- Wittmann, F.H., 1982. Creep and shrinkage mechanisms. In: Bazant, Z.P., Wittmann, F.H. (Eds.), *Creep and Shrinkage in Concrete Structures*. J. Wiley and Sons, pp. 129–161.
- Yip, W.K., Tam, C.T., 1995. Concrete strength evaluation through the use of small diameter cores. *Magazine of Concrete Research* 40 (143), 99–105.
- Yurttaş, I., Burlion, N., Skoczylas, F., 2004a. Experimental characterisation of the drying effect on uniaxial mechanical behavior of mortar. *Materials and Structures* 37, 170–176.
- Yurttaş, I., Burlion, N., Skoczylas, F., 2004b. Triaxial mechanical behavior of mortar: effects of drying. *Cement and Concrete Research* 34, 1131–1143.
- Zhao, H., Gary, G., 1996. On the use of SHPB techniques to determine the dynamic behavior of materials in the range of small strains. *International Journal of Solids and Structures* 33 (23), 3363–3375.
- Zukas, J.A., 1992. *Penetration and Perforation of Solids*. Impact Dynamics. Krieger Publishing Company.